A Biophysical Investigation of Recombinant Hemoglobins with Aromatic B10 Mutations in the Distal Heme Pockets[†,‡]

Mary Ellen Wiltrout, Janel L. Giovannelli, Virgil Simplaceanu, Jonathan A. Lukin,[§] Nancy T. Ho, and Chien Ho*

Department of Biological Sciences, Carnegie Mellon University, Pittsburgh, Pennsylvania 15213

Received August 9, 2004; Revised Manuscript Received March 7, 2005

ABSTRACT: This study examines the structural and functional effects of amino acid substitutions in the distal side of both the α- and β-chain heme pockets of human normal adult hemoglobin (Hb A). Using our *Escherichia coli* expression system, we have constructed four recombinant hemoglobins: rHb(αL29F), rHb(αL29W), rHb(βL28F), and rHb(βL28W). The α29 and β28 residues are located in the B10 helix of the α- and β-chains of Hb A, respectively. The B10 helix is significant because of its proximity to the ligand-binding site. Previous work showed the ability of the L29F mutation to inhibit oxidation. rHb(αL29W), rHb(βL28F), and rHb(βL28W) exhibit very low oxygen affinity and reduced cooperativity compared to those of Hb A, while the previously studied rHb(αL29F) exhibits high oxygen affinity. Proton nuclear magnetic resonance spectroscopy indicates that these mutations in the B10 helix do not significantly perturb the $\alpha_1\beta_1$ and $\alpha_1\beta_2$ subunit interfaces, while as expected, the tertiary structures near the heme pockets are affected. Experiments in which visible spectrophotometry was utilized reveal that rHb(αL29F) has equivalent or slower rates of autoxidation and azide-induced oxidation than does Hb A, while rHb(αL29W), rHb(βL28F), and rHb(βL28W) have increased rates. Bimolecular rate constants for NO-induced oxidation have been determined using a stopped-flow apparatus. These findings indicate that amino acid residues in the B10 helix of the α- and β-chains can play different roles in regulating the functional properties and stability of the hemoglobin molecule. These results may provide new insights for designing a new generation of hemoglobin-based oxygen carriers.

Human adult hemoglobin (Hb A)[1] consists of two α-chains with 141 amino acid residues each and two β-chains with 146 amino acid residues each that form a tetrameric protein molecule (*1*). To investigate the structural and functional properties of Hb, our laboratory has developed an *Escherichia coli* expression system to produce authentic Hb A and recombinant hemoglobins (rHbs) in good yields (*2, 3*). Since the supply of donated blood is limited, recombinant hemoglobin research is important for development and possible applications as a hemoglobin-based oxygen carrier (HBOC) or in Hb therapeutics in a blood substitute system. Our laboratory has designed rHbs that exhibit low oxygen affinity and high cooperativity, properties of interest for a HBOC (*4*−*9*).

Hemoglobin in its natural cellular environment is exposed to allosteric effectors such as 2,3-bisphosphoglycerate (2,3-BPG) that decrease oxygen affinity (*1*). Under extracellular conditions, as in an HBOC, Hb would need to have low oxygen affinity and high cooperativity without the aid of allosteric effectors such as 2,3-BPG. Low-oxygen-affinity mutants of Hb that are found in nature have high rates of autoxidation (heme irons converting from the ferrous to the ferric state) (*6*−*10*). In general, the oxidation rate and oxygen affinity in Hbs are inversely proportional (*11*). This factor presents a problem because Hb is functional only in the reduced, ferrous state.

The distal heme pocket of the B10 helix is located in an area of importance, since previous studies involving L29F mutations at the B10 position in myoglobin (Mb) showed autoxidation inhibition and the ability to lower the rate of oxidation caused by nitric oxide (NO) (*12, 13*). Subsequent work has shown that the L29W mutation in Mb also can reduce the rate of autoxidation and NO-induced oxidation (*14*). The same properties were seen in Hb for the αL29F and αL29W mutants, but not for the βL28F mutant in the B10 position (*14*−*16*). When the αL29F mutation was added to constructed mutants with known low oxygen affinity, rHb(αV96W,βN108K) and rHb(βN108Q), autoxidation and NO-induced oxidation rates decreased, while the low oxygen

[†] This work is supported by research grants from the National Institutes of Health (R01HL-24524 and P01HL-71064). M.E.W. was partially supported by a Beckman Scholars Award from the Beckman Foundation (2003−2004) and through funding from the Undergraduate Science Education Program of the Howard Hughes Medical Institute (2002).

[‡] The preliminary results of this work were presented at the 2003 and 2004 annual meetings of the Biophysical Society.

* To whom correspondence should be addressed: Department of Biological Sciences, Carnegie Mellon University, 4400 Fifth Ave., Pittsburgh, PA 15213. Telephone: (412) 268-3395. Fax: (412) 268-7083. E-mail: chienho@andrew.cmu.edu.

[§] Present address: University Health Network, MBRC, University of Toronto, Toronto, ON M5G2C4, Canada.

[1] Abbreviations: Hb A, human normal adult hemoglobin; rHb, recombinant hemoglobin; HBOC, hemoglobin-based oxygen carrier; HbO_2, oxyhemoglobin; deoxy-Hb, deoxyhemoglobin; HbCO, carbonmonoxyhemoglobin; met-Hb, methemoglobin; azidomet-Hb, azidomethemoglobin; cyanomet-Hb, cyanomethemoglobin; Mb, myoglobin; NO, nitric oxide; CO, carbon monoxide; 2,3-BPG, 2,3-bisphosphoglycerate; P_{50}, partial O_2 pressure at 50% saturation; n_{50}, Hill coefficient at 50% O_2 saturation; EDTA, ethylenediaminetetraacetic acid; NMR, nuclear magnetic resonance; DSS, 2,2-dimethyl-2-silapentane-5-sulfonate; k_{auto}, autoxidation rate; k_{az}, azide-induced oxidation rate; $k'_{ox,NO}$, bimolecular rate constant for NO-induced oxidation.

10.1021/bi048289a CCC: $30.25
Published on Web 04/23/2005

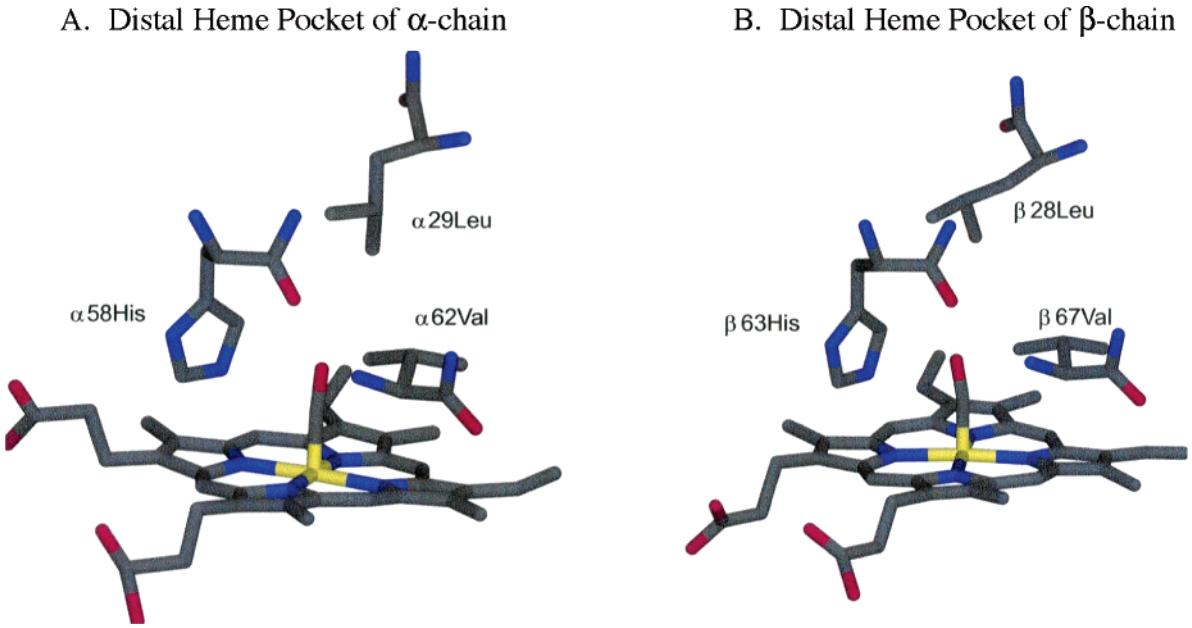

FIGURE 1: Illustration of the location of the B10 mutation target sites (α29Leu and *β*28Leu) relative to the heme pockets of the α-chain (A) and *β*-chain (B) of HbCO A, prepared using MOLMOL (*57*). Coordinates of HbCO A (R2) were obtained from Protein Data Bank entry 1BBB.

affinity was maintained as previously reported (*6*−*8*). The rate of azide-induced oxidation, a reaction in which oxidation is promoted by anionic azide, is lower for rHb(αL29F) than for Hb A (*7*, *8*).

NO scavenging has been reported to be directly related to the hypertension resulting from the use of extracellular HBOCs (*16*). This study additionally concluded that the NO-induced oxidation rates were related to the degree of hypertension, suggesting that Hbs with lower rates of NO-induced oxidation may reduce the hypertension effect. Since the major cause of NO scavenging is the NO dioxygenation by MbO_2 and HbO_2, finding rHbs with low NO reactivity was also supported by Dou et al. (*17*). Therefore, studying the NO-induced oxidation properties of distal heme pocket rHbs is critical due to the previous findings involving these mutations in Mb and Hb.

To further examine the structural and functional properties of rHbs with mutations in the distal heme pockets of the α- and *β*-chains, rHb(αL29W), rHb(*β*L28F), and rHb(*β*L28W) have been constructed in our laboratory in addition to the previously studied rHb(αL29F) (*7*, *8*). Figure 1 shows the proximity of the α29 (B10) and *β*28 (B10) amino acid residues of Hb A to the distal heme pockets of both the α- and *β*-chains, the area of ligand binding. One can also see how substitutions of large amino acids such as Phe or Trp for Leu in these positions could affect ligand binding in the heme pocket. Our laboratory has selected rHb(αL29F), rHb(αL29W), rHb(*β*L28F), and rHb(*β*L28W) to test the oxygen affinity, cooperativity, and structural properties of distal heme pocket mutations in the B10 helix that could have some effect on autoxidation, azide-induced oxidation, and NO-induced oxidation rates relative to Hb A. This paper investigates the similarities and differences among these four rHbs with amino acid substitutions in the distal heme pocket, between the same mutations on the α-chain versus *β*-chain, and between the substitution of Phe versus Trp in the B10 position of the α- and *β*-chains.

MATERIALS AND METHODS

Expression of rHbs. The *E. coli* Hb expression plasmid, pHE2, was designed in our laboratory as previously described by Shen et al. (*2*). Plasmids pHE284, pHE285, pHE286, and pHE287, which expressed the distal heme pocket α29Leu → Phe, α29Leu → Trp, *β*28Leu → Phe, and *β*28Leu → Trp mutations, respectively, were derived from pHE2 with the QuickChange site-directed mutagenesis kit (Stratagene) and with appropriate oligonucleotides containing the expected mutated codons. Previous work by our laboratory has detailed the construction of pHE284 for the expression of rHb(αL29F) (*8*).

Materials. Hb A was isolated and purified from human normal blood samples obtained from the local blood bank using the standard procedures in our laboratory (*2*). Chemicals and restriction enzymes were purchased from Fisher, Sigma, Bio-Rad, Boehringer Mannheim, New England Biolabs, Pharmacia, Promega, and United States Biochemical Corp., Inc.

Culture Growth. Plasmids pHE284, pHE285, pHE286, and pHE287 were each transformed separately into *E. coli* strain JM109. Growth of *E. coli* cells was in rich, Terrific Broth (TB) media in a 5 L Microferm fermentor (New Brunswick Scientific, model BioFlo 3000) at 32 °C until the optical density reached ∼10 at 600 nm. More recently, growth was in a 20 L fermentor (B. Braun Biotech International, model Biostat C) following the same procedure. Isopropyl *β*-thiogalactopyranoside was then added at a concentration of 24 mg/L to induce the expression of the rHbs. After the addition of hemin (25 mg/L), growth continued for at least four additional 4 h. Harvesting was accomplished through centrifugation. Cell paste was stored at −80 °C until it was needed.

Purification. Cell paste was suspended in 3 mL of lysis buffer [40 mM Tris (pH 8.6) and 1 mM benzamidine (protease inhibitor)] per gram of cell paste. Unless otherwise stated, the sample was always in a CO environment and

temporarily stored or centrifuged at 4 °C. For all rHbs, cells were lysed using a high-pressure homogenizer (Avestin, EmulsiFlex-C5). After centrifugation for 2.5 h at 12 000 rpm in a Beckman JA-14 rotor, the supernatant was kept in the 30 °C incubator overnight. Polyethyleneimine was added to a concentration of 0.5%. The sample was centrifuged at 8000 rpm for 30 min to pellet the precipitated nucleic acids. The sample was put through a Millipore Minitan Acrylic Ultrafiltration system and was then dialyzed against a buffer solution containing 20 mM Tris-HCl (pH 8.5) and 0.5 mM EDTA overnight with one exchange. The rHb was collected after use of a Q-Sepharose Fast-Flow column, then oxidized with $K_3Fe(CN)_6$, reduced to the deoxy form with sodium dithionite, and converted into the CO form as detailed by Shen et al. (*2*, *3*). The rHb was purified further via fast protein liquid chromatography (FPLC) using a Mono S column.

Characterization of rHbs. To confirm that the correct mutations and efficient cleavage of the N-terminal methionine were obtained in the purified rHbs, mass spectrometry and Edman degradation were performed on the proteins as described by Shen et al. (*2*). The VG Quattro-Bio-Q mass spectrometer (Fisons Instruments, VG Biotech, Altrincham, U.K.) was used for electrospray ionization mass spectrometric analyses. Automated cycles of Edman degradation were accomplished with an Applied Biosystems gas/liquid-phase sequencer (model 470/900A) equipped with an on-line phenylthiohydantoin amino acid analyzer (model 120A). All of the rHbs examined in this study had the correct molecular weights and less than 5% N-terminal methionine.

Oxygen Binding Properties. A Hemox Analyzer (TCS Medical Products, Huntington Valley, PA) was used to measure oxygen dissociation curves. As previously described, the experiments were run at 29 °C as a function of pH in 0.1 M sodium phosphate buffer and 0.1 mM hemoglobin (in terms of heme) (*2*, *3*). The addition of a methemoglobin (met-Hb) reductase system was designed to slow the formation of met-Hb (*18*). Using a nonlinear least-squares procedure, results were calculated by fitting the Adair equations to each equilibrium oxygen binding curve. Oxygen affinity was determined by P_{50} values taken at 50% O_2 saturation. Hill coefficients, n_{50}, were calculated from the slope of the Hill plot at 50% saturation as a measure of cooperativity. The P_{50} values (in millimeters of Hg) are given with an accuracy of ±5%. The n_{50} values are reported with an accuracy of ±10%.

Autoxidation of rHbs. Autoxidation experiments mostly followed those used by Jeong et al. (*8*) that were modified from those of Carver et al. (*12*). rHbs in the CO form were converted to $rHbO_2$ by passing O_2 gas through a rotary flask containing the rHbCO solution, under lamp light and in an ice bath, for ~1 h. To make certain that there was complete conversion to $rHbO_2$, the optical spectrum was checked (*2*, *3*). The autoxidation reaction took place in a 3 mL cuvette containing 0.1 M sodium phosphate buffer with 1.0 mM EDTA at pH 7.0 and 25 °C. The temperature was maintained with a Single Cell Peltier (Varian) device. The concentration of $rHbO_2$ in terms of heme was 60 μM (an optical density of ~1.0 at 577 nm). The Cary 50 UV−visible spectrophotometer (Varian) recorded the absorbances at 560, 577, and 630 nm every 15 min for 7 h. Concentrations of oxy-Hb, met-Hb, and hemichrome were determined from these absorbances and their millimolar extinction coefficients as previously described (*8*, *19*−*21*). The millimolar extinction coefficients were as follows: $\epsilon_{560} = 36.5$ mM^{-1} cm^{-1}, $\epsilon_{577} = 66$ mM^{-1} cm^{-1}, and $\epsilon_{630} = 1.0$ mM^{-1} cm^{-1} for oxy-Hb, $\epsilon_{560} = 16.2$ mM^{-1} cm^{-1}, $\epsilon_{577} = 16.2$ mM^{-1} cm^{-1}, and $\epsilon_{630} = 16$ mM^{-1} cm^{-1} for Met-Hb, and $\epsilon_{560} = 36.5$ mM^{-1} cm^{-1}, $\epsilon_{577} = 28.6$ mM^{-1} cm^{-1}, and $\epsilon_{630} = 3.9$ mM^{-1} cm^{-1} for hemichrome. Using those extinction coefficients, $A_{560} = 36.5$[oxy-Hb] + 16.2[met-Hb] + 36.5[hemichrome], $A_{577} = 66$[oxy-Hb] + 16.2[met-Hb] + 28.6[hemichrome], and $A_{630} = 1.0$[oxy-Hb] + 16[met-Hb] + 3.9[hemichrome]. These equations were rearranged to give [oxy-Hb] $= -19.9A_{560} + 26.3A_{577} - 6.45A_{630}$, [met-Hb] $= -11.4A_{560} + 5.3A_{577} + 68.8A_{630}$, and [oxy-Hb] $= 51.9A_{560} - 28.4A_{577} - 24.1A_{630}$ for determining the concentration of each Hb species. The logarithm (base 10) of percent oxy-Hb was plotted as a function of time, and exhibited linearity. Using linear regression, the slope corresponded to the first-order rate constant of autoxidation for the initial rate.

Azide-Induced Oxidation of rHbs. Experiments for the azide-induced oxidation were modified from those previously described (*8*, *22*, *23*). As with autoxidation, rHb was converted from rHbCO to $rHbO_2$. A 3 mL cuvette contained 60 μM oxy-Hb in a 0.1 M sodium phosphate and 1.0 mM EDTA buffer (pH 7.0) and was kept at 25 °C. Immediately before the absorbances were recorded, sodium azide was added at a concentration of 0.1 M. The absorbances were measured at 577 and 630 nm every 15 min for the first 7 h. The millimolar extinction coefficients as follows: were $\epsilon_{577} = 66$ mM^{-1} cm^{-1} and $\epsilon_{630} = 1.0$ mM^{-1} cm^{-1} for oxy-Hb and $\epsilon_{577} = 33.48$ mM^{-1} cm^{-1} and $\epsilon_{630} = 7.9$ mM^{-1} cm^{-1} for azidomet-Hb (*8*, *23*, *24*). From these extinction coefficients, $A_{577} = 66$[oxy-Hb] + 33.48[azidomet-Hb] and $A_{630} = 1.0$[oxy-Hb] + 7.9[azidomet-Hb]. The concentrations of oxy-Hb and azidomet-Hb were then determined from the following equations: [oxy-Hb] $= 16.2A_{577} - 68A_{630}$ and [azidomet-Hb] $= -2.05A_{577} + 135A_{630}$. The log of percent oxy-Hb was plotted as a function of time to show the linearity of the initial rate as expected for first-order kinetics. The initial rate was found from the slope of the line as derived by linear regression.

NO-Induced Oxidation Measurements. NO-induced oxidation was assessed on an Olis stopped-flow apparatus (Olis, Bogart, GA) with a dead time of at least 3 ms as described by Tsai et al. (*7*). Rapid mixing reactions took place at 20 °C, the temperature maintained by a circulating water bath. To ensure anaerobic conditions, the day before experiments were carried out, the chambers of the stopped-flow apparatus were loaded with a 10 mg/10 mL dithionite solution of degassed 0.1 M sodium phosphate buffer at pH 8.5. The water that was circulating through the stopped-flow apparatus for temperature control was saturated with argon gas overnight. On the day of the experiment, the dithionite buffer solution was thoroughly flushed out of the sample chambers with argon-gassed 0.1 M sodium phosphate buffer at pH 7.0. No buffer solutions used in the experiments contained dithionite. Argon gas continually ran through the water bath during this time and during experiments. The absorbance was measured at 402 nm to detect the formation of methemoglobin (met-Hb) as a result of mixing oxy-Hb with anaerobic NO solutions. The protein concentration was kept at 0.4 μM heme before mixing to have a pseudo-first-order approxima-

tion. The NO concentrations that were selected were less than 5 μM after mixing due to the very fast rate of the reaction. Otherwise, the reaction would go to completion before the dead time for the apparatus. Observed rates are based on the average of 10−14 reactions to improve the signal-to-noise ratio. As previously reported, the bimolecular rate constant was in the range of 30−50 μM^{-1} s^{-1} for Hb A depending on the nature of the buffer and temperature (*14*, *15*, *25*). Multiple NO concentrations were used to calculate the bimolecular rate constant. Through an iterative nonlinear least-squares algorithm, the traces were fitted to a single-exponential expression to determine the observed rate. The bimolecular rate constants were determined to be the observed rate divided by the concentration of NO ($k'_{ox,NO} = k_{obs}/[NO]$).

Structural Studies with ^{1}H NMR Spectroscopy. To detect changes in the tertiary or quaternary structure of the rHbs, ^{1}H NMR spectra were recorded on a Bruker Avance DRX-300 NMR spectrometer. Samples consisted of aqueous solutions of hemoglobin at a concentration of 5% (3.1 mM in terms of heme) in 0.1 M sodium phosphate buffer at pH 7.0 in 95% water and 5% deuterium oxide (D_2O) and were assessed at 29 °C. A jump-and-return pulse sequence was used to suppress the water signal (*26*). ^{1}H chemical shifts were indirectly referenced to the methyl proton resonance of the sodium salt of 2,2-dimethyl-2-silapentane-5-sulfonate (DSS) through use of the internal reference of the water signal at 4.76 ppm downfield of DSS at 29 °C.

RESULTS

Oxygen Binding Properties. Figure 2 shows the oxygen binding properties of Hb A and four rHbs, rHb(αL29F), rHb(αL29W), rHb(βL28W), and rHb(βL28F), compared to the properties of Hb A in 0.1 M sodium phosphate buffer as a function of pH at 29 °C. Figure 2A shows the percent of O_2 saturation of Hb A and the four rHbs as a function of partial pressure of O_2 in 0.1 M sodium phosphate at pH 7.4 and 29 °C, illustrating the differences among the four rHbs and Hb A. Panels B and C of Figure 2 and Table 1 show the oxygen binding properties of of the four rHbs as compared to those of Hb A. The oxygen affinity results in panels A and B of Figure 2 show that rHb(αL29W) has a low oxygen affinity (i.e., high P_{50} values), but rHb(αL29F) shows a high oxygen affinity with low P_{50} values as previously reported by Jeong et al. (*8*). The mutations on the β-chain, however, exhibit a low oxygen affinity for both rHb(βL28F) and rHb(βL28W). These findings indicate different functional properties between the same mutations (Leu → Phe) on the α-chain versus the β-chain. Different mutations (Leu → Phe and Leu → Trp) at the same location on the α-chain cause opposite oxygen affinity results, while the same two mutations on the β-chain in the equivalent location produce similar oxygen affinity results. As seen in Figure 2C, the Hill coefficients (n_{50}), a measure of cooperativity, decrease somewhat for all four rHbs as a result of the mutations in the distal heme pocket. The P_{50} values at pH 7.4 for Hb A, rHb(αL29F), rHb(αL29W), rHb(βL28F), and rHb(βL28W) are 9.3, 4.9, 31.5, 35.7, and 64.6 mmHg, respectively, and the Hill coefficients (n_{50}) are 3.1, 3.0, 2.2, 2.6, and 1.7, respectively (Table 1). The oxygen binding properties of rHb(βL28W) were difficult to obtain because of its propensity to convert easily to met-Hb, even in the presence of a met-Hb reductase system (*18*).

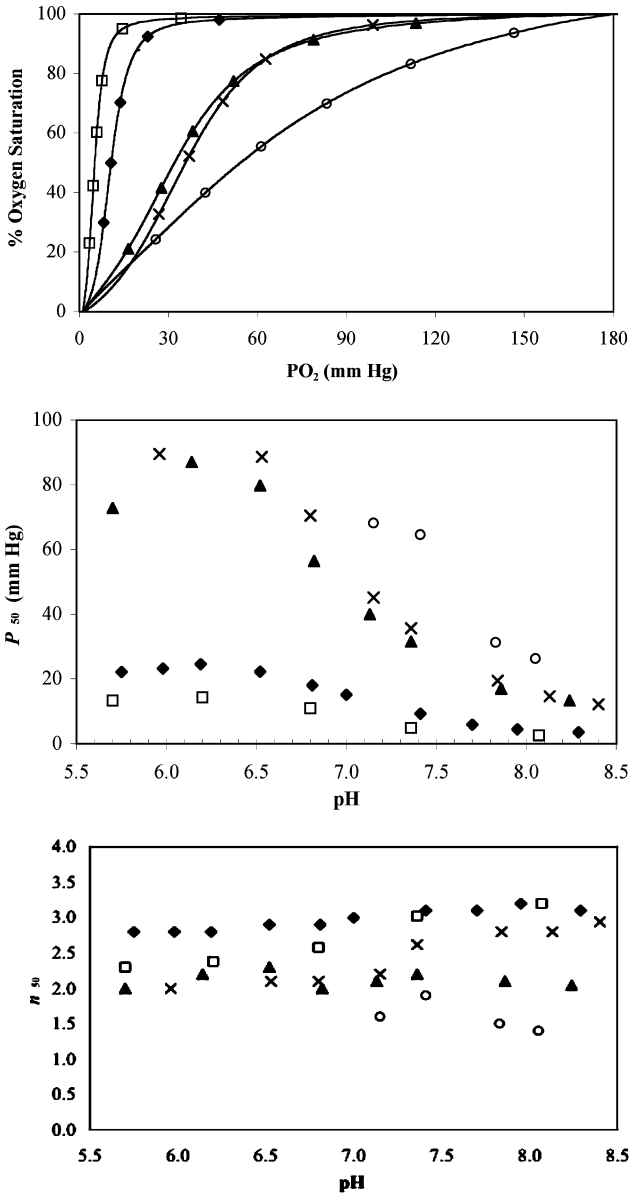

FIGURE 2: Oxygen binding properties of Hb A and rHbs in 0.1 M sodium phosphate buffer as a function of pH at 29 °C. (A) Percent of O_2 saturation as a function of the partial pressure of O_2 at pH 7.4, (B) oxygen affinity as a function of pH, and (C) Hill coefficient as a function of pH: (◆) Hb A, (□) rHb(αL29F), (▲) rHb(αL29W), (×) rHb(βL28F), and (○) rHb(βL28W).

Bohr Effect. Table 2 shows the values calculated for the Bohr effect in 0.1 M sodium phosphate buffer at 29 °C from the data displayed in Table 1. The alkaline Bohr effect causes the oxygen affinity to decrease in Hb A due to an increase in the concentration of H^+ ions (lowering the pH). Using the linkage equation $[\Delta H^+ = -\partial(\log P_{50})/\partial(\mathrm{pH})]$ for calculations, the data in Table 2 represent the number of Bohr protons released upon oxygenation per heme (*27*, *28*). The values in Table 2 suggest there is little difference in the Bohr effect among the four rHbs and Hb A.

Autoxidation. Table 3 gives the calculated rate constants for autoxidation in 0.1 M sodium phosphate buffer at pH 7.0 and 25 °C. These rates were calculated from readings taken by visible spectrophotometry during the first 7 h to detect the autoxidation of oxy-Hb. It has been reported that

Table 1: Oxygen Binding Data Given as the Oxygen Affinity (P_{50}) and Hill Coefficient at 50% Saturation (n_{50}) in 0.1 M Sodium Phosphate Buffer as a Function of pH at 29 °C in the Presence of a Met-Hb Reductase System (*18*)

hemoglobin	pH	P_{50}	n_{50}	hemoglobin	pH	P_{50}	n_{50}
Hb A	6.52	22.3	2.9	rHb(βL28F)	6.53	88.6	2.1
	6.81	18.1	2.9		6.80	70.5	2.1
	7.00	15.1	3.0		7.15	45.1	2.2
	7.41	9.3	3.1		7.36	35.7	2.6
	7.70	5.9	3.1		7.84	19.5	2.8
	7.95	4.5	3.2		8.13	14.7	2.8
	8.29	3.6	3.1	rHb(βL28W)	7.15	68.1	1.6
rHb(αL29F)	6.20	14.3	2.4		7.41	64.6	1.7
	6.80	10.9	2.6		7.83	31.3	1.5
	7.36	4.9	3.0		8.05	26.3	1.4
	8.07	2.6	3.2				
rHb(αL29W)	6.52	79.8	2.3				
	6.82	56.4	2.0				
	7.13	40.0	2.1				
	7.36	31.5	2.2				
	7.86	17.0	2.1				
	8.24	13.3	2.0				

Table 2: Bohr Effect of Hb A and rHbs in 0.1 M Sodium Phosphate Buffer at 29 °C[a]

hemoglobin	$-\Delta(\log P_{50})/\Delta$pH
Hb A	0.46 (pH 6.52−8.29)
rHb(αL29F)	0.39 (pH 6.20−8.07)
rHb(αL29W)	0.45 (pH 6.52−8.24)
rHb(βL29F)	0.49 (pH 6.53−8.13)
rHb(βL28W)	0.46 (pH 7.15−8.05)

[a] Best estimate values were determined from the pH range in parentheses in the presence of a met-Hb reductase system (*18*).

Table 3: Autoxidation and Azide-Induced Oxidation Rate Constants Measured at pH 7.0 and 25 °C in 0.1 M Sodium Phosphate Buffer

hemoglobin	k_{auto} (h^{-1})[a]	k_{az} (h^{-1})[b]
Hb A	0.0009 ± 0.0005	0.052 ± 0.007
rHb(αL29F)	0.0009 ± 0.0002	0.014 ± 0.002
rHb(αL29W)	0.007 ± 0.001	0.06 ± 0.01
rHb(βL29F)	0.017 ± 0.002	0.09 ± 0.01
rHb(βL29W)	0.019 ± 0.002	0.21 ± 0.04

[a] k_{auto} is the autoxidation rate. [b] k_{az} is the azide-induced oxidation rate.

the autoxidation reaction of oxy-Hb A is biphasic with the fast autoxidation due to the α-chain and the slower one due to the β-chain (*29*−*31*). We too have observed this biphasic nature of the autoxidation reaction for both Hb A and rHbs (results not shown), with the rates for HbO_2 A differing by a factor of approximately 2. However, we have restricted our attention to the autoxidation reaction during the first 7 h in our studies and approximated it by a monoexponential process with an effective average rate constant over this time interval. The decrease in percentage of ferrous-Hb as a function of time (t) at pH 7.0 can then be written as $[\text{ferrous-Hb}]_t = [\text{ferrous-Hb}]_{t=0} \exp(-k_{auto}t)$ as previously described by Jeong et al. (*8*). The autoxidation rate constant is represented by the variable k_{auto} and represents the average value during the first 7 h of the reaction. The k_{auto} value for our HbO_2 A under our experimental condition of 0.1 M sodium phosphate at pH 7.0 and 25 °C is 0.0009 h^{-1}. The corresponding values for HbO_2 A reported by Shikama and co-workers (*29*, *30*) are 0.078 h^{-1} (the fast phase due to the α-chain) and 0.011 h^{-1} (the slow phase due to the β-chain) in 0.1 M 2-(*N*-morpholino)ethanesulfonic acid buffer and 1 mM EDTA at pH 6.5 and 35 °C. They further reported that the rates of autoxidation for HbO_2 A decrease strongly from pH 5 to 7 and become monophasic and identical from pH 8 to 10 and that the difference in the autoxidaton rates between the fast and slow phases is a factor of ∼2.8 at pH 7.0 (*30*). Considering the differences in experimental conditions (temperature and buffer) between our study and those carried out by Shikama and co-workers, our k_{auto} value for HbO_2 A is qualitatively similar to that reported by them.

Table 4: NO-Induced Oxidation Rates Measured at pH 7.0 and 20 °C in 0.1 M Argon-Saturated Sodium Phosphate Buffer

hemoglobin	$k'_{ox,NO}$ (μM^{-1} s^{-1})[a]	hemoglobin	$k'_{ox,NO}$ (μM^{-1} s^{-1})[a]
Hb A	20 ± 2	rHb(βL29F)	15 ± 2
rHb(αL29F)	2.0 ± 0.2	rHb(βL28W)	13 ± 1
rHb(αL29W)	9.2 ± 0.8		

[a] $k'_{ox,NO}$ is the second-order rate constant for NO-induced oxidation.

The αL29F mutation in the B10 helix had previously been shown to inhibit autoxidation and NO-induced oxidation, but to increase the oxygen affinity (*8*). The oxidation rates for Hb A and for the four mutant rHbs were measured using the procedures of our laboratory (*7*, *8*). According to the calculated rate constants in Table 3, rHb(αL29F) exhibits the same rate of autoxidation as Hb A, while rHb(αL29W) undergoes autoxidation approximately 7.8 times faster than Hb A. The rate constants of autoxidation for rHb(βL28F) and rHb(βL28W) are similar to each other, are approximately 2.6 times greater than the rate constant of rHb(αL29W), and are approximately 20 times greater than the rate constants of Hb A or rHb(αL29F). The rate constant of autoxidation for Hb A is 20 times slower than the value reported by Jeong et al. (*8*) under the same conditions. The rate for autoxidation of rHb(αL29F) was found to be 10 times slower than that reported by Jeong et al. (*8*). Since these new rate constants have reasonable standard deviations and those differences lie outside of the standard deviations, the differences could be due to the use of a newer, better spectrophotometer, better temperature control, or another source of systematic errors between the two sets of data.

Azide-Induced Oxidation. The calculated rate constants for azide-induced oxidation in 0.1 M sodium phosphate buffer at pH 7.0 and 25 °C are listed in Table 3. As described by Jeong et al. (*8*), oxy-Hb converts into the azidomet form of Hb when placed in a sodium azide solution. As with autoxidation, the percentage of ferrous Hb is treated as having a monoexponential relationship with respect to time (t) for an easy calculation of the rate constnant of azide-induced oxidation (k_{az}). For rHb(αL29F), the azide-induced oxidation rate constant is almost 4 times slower than that of Hb A. The rate constants of azide-induced oxidation for rHb(αL29W), rHb(βL28F), and rHb(βL28W) are 1.2, 1.7, and 4 times faster than that for Hb A, respectively (Table 3). Despite some variations from the values reported by Jeong et al. (*8*), the results confirm previous findings that the Leu → Phe mutation on the α-chain inhibits azide-induced oxidation. The rate constants in Table 3 show that no other distal heme pocket mutant that was tested possesses the ability to inhibit oxidation as strongly as rHb(αL29F).

NO-Induced Oxidation. Table 4 gives the bimolecular rate constants ($k'_{ox,NO}$) for the NO-induced oxidation obtained in

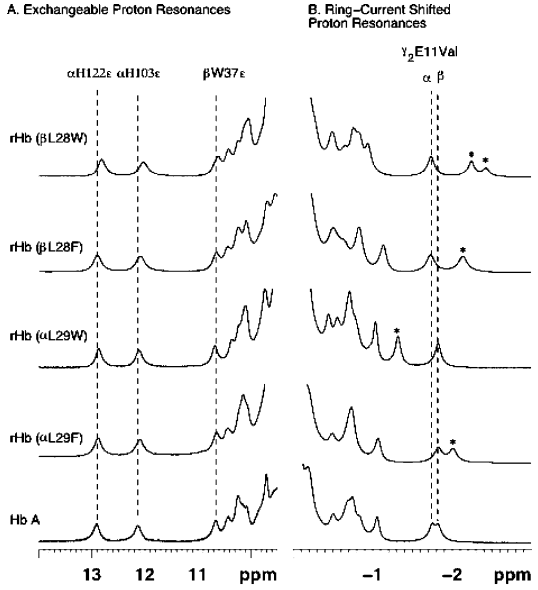

FIGURE 3: ^{1}H NMR spectra (300 MHz) of the CO form of rHbs in 95% H_2O, 5% D_2O, 0.1 M sodium phosphate buffer at pH 7.0 and 29 °C: (A) exchangeable proton resonances and (B) ring current-shifted proton resonances. Asterisks indicate shifted resonances. The spectra for rHb(αL29F) were redrawn from the data of Jeong et al. (*8*).

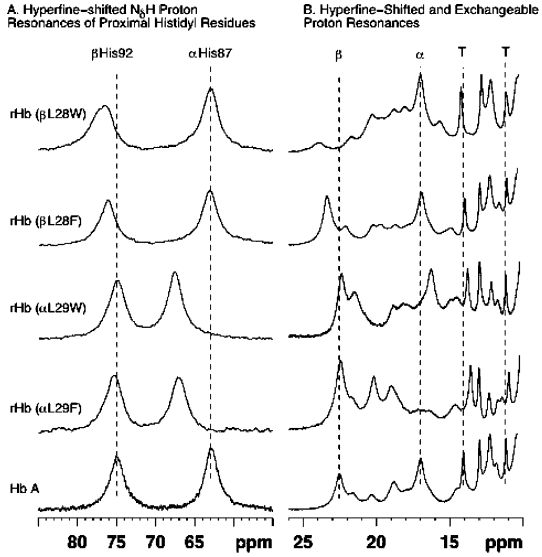

FIGURE 4: ^{1}H NMR spectra (300 MHz) of the deoxy form of Hb A and rHbs in 95% H_2O, 5% D_2O, 0.1 M sodium phosphate buffer at pH 7.0 and 29 °C: (A) hyperfine-shifted $N_\delta H$ proton resonances of proximal histidyl residues and (B) hyperfine-shifted and exchangeable proton resonances. The spectra for rHb(αL29F) were redrawn from the data of Jeong et al. (*8*).

0.1 M sodium phosphate buffer at pH 7.0 and 20 °C. The NO-induced oxidation of Hb A has a second-order rate constant of 20 μM^{-1} s^{-1}, which is smaller than the values (30−50 μM^{-1} s^{-1}) for Hb A reported by Eich et al. (*15*) under different experimental conditions. All the distal heme pocket mutations that were tested show inhibition of NO-induced oxidation compared to the oxidation seen in Hb A. The NO-induced oxidation of Hb A and our rHbs should be biphasic as previously reported in ref *15* and by us (*7*). Because of limitations of our stopped-flow apparatus, we likely missed the faster phase of the reaction. The NO-induced oxidation rate constants for Hb A and rHb(αL29F) are very similar to the rates found by Tsai et al. (*7*). The bimolecular rate constants of NO-induced oxidation for Mbs were found to be much slower than that of the wild type for the L29F and L29W mutations (*14*, *15*), a trend also seen in these results for rHbs. However, the β-chain mutation of Leu → Phe in the B10 helix was previously found to produce little to no inhibition of NO-induced oxidation in hemoglobin (*15*). The bimolecular rate constants in Table 4 for rHb(βL28F) and rHb(βL28W) show some inhibition of the NO-induced oxidation. These results do not follow the trend found for auto- and azide-induced oxidation properties of the β-chain rHbs shown in Table 3, which have faster rates of oxidation than Hb A. Still, the same pattern exists in Tables 3 and 4 for all three types of oxidation studied in that both α-chain B10 mutant rHbs have slower oxidation rates than both β-chain B10 mutant rHbs.

Structural Properties. As previously shown, ^{1}H NMR spectroscopy serves as an excellent tool for investigating changes in the tertiary and quaternary structures of hemoglobin (*32*). Figures 3 and 4 show the 300 MHz ^{1}H NMR spectra of Hb A and the four B10 mutant hemoglobins in 0.1 M sodium phosphate buffer at pH 7.0 and 29 °C in the CO and deoxy forms.

NMR Spectra of Hemoglobins in the CO Form. The resonances between 9 and 14 ppm arise mainly from the exchangeable protons in the intersubunit interfaces and from the heme mesoprotons (Figure 3A). The resonances at 12.9 and 12.1 ppm from DSS have been assigned to $NH_{\epsilon 1}$ of the side chains of α122His and α103His H-bonded to β35Tyr and β131Gln, respectively (*33*−*35*), in the $\alpha_1\beta_1$ interface. The resonance at 10.6 ppm has been assigned to the exchangeable, H-bonded $NH_{\epsilon 1}$ of β37Trp, an intersubunit contact site in the $\alpha_1\beta_2$ interface of HbCO A (*34*, *36*). The resonance at 12.1 ppm in HbCO A is shifted slightly upfield in rHbCO(αL29F) and in rHbCO(βL28F), while the resonance at 12.9 ppm is not affected in these mutants.

The resonance at 12.9 ppm is slightly shifted upfield in rHb(αL29W), while the resonance at 12.1 ppm is not affected. Both $\alpha_1\beta_1$ interface histidyl resonances are shifted upfield noticeably in rHb(βL28W). We interpret these results as an indication of no significant perturbation of the average quaternary structure at the $\alpha_1\beta_1$ interface of the B10 mutant hemoglobins, with the exception of rHb(βL28W). The structural marker of the $\alpha_1\beta_2$ interface at 10.6 ppm does not show changes in chemical shift, indicating that there is no detectable change in the quaternary structure at the $\alpha_1\beta_2$ interface either.

Figure 3B shows the nonexchangeable ring current-shifted proton resonances from 0 to −3 ppm from DSS. These resonances provide information about the tertiary structure of the heme pocket. The resonances at −1.75 and −1.82 ppm have been assigned to the γ_2-CH_3 group of E11Val of the α- and β-chains of HbCO A, respectively (*37*, *38*). For each B10 mutant, the E11Val methyl resonance of the corresponding chain is shifted to a distinct position, while the resonance of the native chain is not affected. Other resonances in the region from 0 to −1.2 ppm are also affected, but we do not have the resonance assignments for them yet. The E11Val methyl peak in rHb(αL29F) is shifted upfield by 0.26 ppm to −2.01 ppm. In rHbCO(αL29W), this resonance is shifted downfield by 0.43 ppm to −1.32 ppm. The βL28F mutant exhibits a significant, 0.31 ppm, upfield shift to −2.13 ppm, while the βL28W mutant exhibits two

shifted resonances of unequal intensities at −2.24 and −2.42 ppm, with much larger upfield shifts of 0.42 and 0.6 ppm, indicative of a degree of structural inhomogeneity in the distal heme pocket of this mutant.

NMR Spectra of Hemoglobins in the Deoxy Form. The region between 60 and 80 ppm from DSS in Figure 4A shows the hyperfine-shifted proton resonances of the $N_\delta H$ exchangeable proton of proximal histidine residues αHis87 at 63 ppm and *β*His92 at 76 ppm for Hb A in the deoxy form (*39*, *40*). These are markers of the tertiary structure of the proximal heme pockets. It is apparent that the B10 mutations of the α-chain induce a downfield shift of ∼4 ppm for αL29F and ∼5 ppm for αL29W, while the *β*-chain peak is unaffected. In the case of B10 mutations of the *β*-chain, there is a small, 1 ppm, downfield shift for *β*L28F, while *β*L28W shows a larger, 2 ppm, downfield shift and also a broadening consistent with a structural inhomogeneity of the proximal heme pocket as well for this mutant. The α-chain proximal heme pocket does not seem to be affected by the mutations in the *β*-chain.

The spectral region between 10 and 25 ppm downfield from DSS (Figure 4B) displays the hyperfine-shifted resonances of the porphyrin ring and of amino acid residues situated in or near the heme pocket, as well as the exchangeable proton resonances of the subunit interfaces of Hb A in the deoxy form (*32*). The resonances downfield of 14 ppm belong to nonexchangeable hyperfine-shifted protons, and some are identified by subunit type (α or *β*). The mutations studied here induce great perturbations in these resonances: the resonance at 17 ppm shifts downfield to 20.5 ppm in rHb(αL29F) and shifts upfield in rHb(αL29W); the resonance at 22.5 ppm shifts to 23.5 ppm for rHb(*β*L28F), while for rHb(*β*L28W) it shifts to ∼24 ppm and broadens.

The resonance at 14.1 ppm has been assigned as the H-bond between α42Tyr and *β*99Asp in the $\alpha_1\beta_2$ interface of deoxy-Hb A (*41*), an important marker of the T-structure of deoxy-Hb A (*42*). This resonance shifts very slightly downfield for rHb(*β*L28W), very slightly upfield for rHb(*β*L28F), somewhat more upfield for rHb(αL29W), and noticeably for rHb(αL29F).

The resonances at 13.0 and 12.2 ppm from DSS in the spectrum of deoxy-Hb A represent the same α122His and α103His resonances, respectively, in the $\alpha_1\beta_1$ interface as for the ligated CO form. There is no apparent shift of these resonances in the mutants. Another T-structure marker is the resonance at 11.2 ppm, representing the exchangeable NH indole proton of *β*37Trp forming an H-bond to α94Asp in the $\alpha_1\beta_2$ interface (*34*, *41*, *43*). There is very little if any shift of this resonance for all mutants except rHb(αL29F), for which there is a slight upfield shift compared to that of Hb A. There appears to be little or no significant perturbation of the quaternary structure of either the $\alpha_1\beta_1$ or $\alpha_1\beta_2$ interface in all four B10 mutants in the deoxy form.

DISCUSSION

This study characterizes the functional and structural properties of four expressed rHbs with mutations at the B10 position of both the α- and *β*-chains. We investigated the consequences of substitutions of Phe or Trp for Leu residues located near the oxygen-binding site in Hb. We are especially interested in whether rHb(αL29W), rHb(*β*L28F), and rHb(*β*L28W), all found to have low oxygen affinity and fairly high cooperativity, would possess the ability to inhibit oxidation like the previously studied rHb(αL29F) (*7*, *8*).

As seen in Figure 2, functional properties of the α-chain differ in comparison to those of the *β*-chain with the same mutations in the B10 position. The high oxygen affinity of rHb(αL29F) contrasts greatly with the very low oxygen affinity exhibited by rHb(*β*L28F). Also, the inhibitory effects of rHb(αL29F) on autoxidation, azide-induced oxidation, and NO-induced oxidation are not seen in rHb(*β*L28F) (Tables 3 and 4). Eich et al. (*15*) reported similar results in that the inhibition of NO-induced oxidation occurred in the α-chain and not the *β*-chain mutations to Phe in the B10 position. rHb(αL29W) differs from rHb(*β*L28W) in its oxidation inhibition, but not oxygen binding properties. Both rHb(αL29W) and rHb(*β*L28W) have very low oxygen affinities, but rHb(αL29W) is more stable against oxidation than rHb(*β*L28W) (Tables 3 and 4).

Our results indicate that amino acid substitutions of Phe and Trp for Leu in the same position on the same chain exhibit different functional properties. Although rHb(*β*L28F) and rHb(*β*L28W) do not behave exactly the same with respect to oxygen binding, rHb(αL29F) and rHb(αL29W) have opposite oxygen affinities. rHb(αL29F) has a high oxygen affinity, while rHb(αL29W) has a very low oxygen affinity as illustrated in panels A and B of Figure 2. However, the effects on oxidation are not conflicting for these two rHbs. In fact, the oxidation properties of rHb(αL29W) most closely resemble those of rHb(αL29F) (Tables 3 and 4). This agrees with previous findings in myoglobin and hemoglobin in which the autoxidation and NO-induced oxidation were inhibited by both of the B10 mutations, L29F and L29W (*14*−*16*). Unlike these α-chain rHbs, the *β*-chain rHbs with mutations in the distal heme pocket share similar functional properties for oxidation and oxygen affinity. Both *β*-chain rHbs have very low oxygen affinities while maintaining cooperativity (Figure 2B,C). The autoxidation and azide-induced oxidation rates are both significantly faster than for Hb A, with the rates for rHb(*β*L28W) being somewhat faster than for rHb(*β*L28F). In general, rHb(*β*L28W) has more problems with met-Hb formation than the other rHbs investigated in this report. The cause for this observation needs further study. A possible hint is the greater perturbation and structural inhomogeneity of the distal heme pocket as evidenced by the changes in the ring current-shifted proton resonances (Figure 3B) and of the hyperfine-shifted resonances (Figure 4A,B).

The oxidation inhibitory effects of rHb(αL29F) have been explained by the ability of the large phenyl ring of Phe to exclude water in the distal heme pocket. The oxygen affinity still remains high due to favorable electrostatic interactions between the bound oxygen and the positive edge of the phenyl ring multipole (*12*, *14*, *17*). When Trp replaces Leu in the B10 position, the even larger indole side chain of Trp can cause steric hindrance with the iron and bound ligand as proposed by Dou et al. (*17*). This could account for the great difference in oxygen affinity between rHb(αL29F) and rHb(αL29W). The side chain of Trp prevents oxygen binding in the distal heme pocket, leading to low oxygen affinity as seen in rHb(αL29W) and rHb(*β*L28W) (Figure 2A,B).

According to this argument, rHb(*β*L28F) should possess high oxygen affinity and inhibitory effects for oxidation due to the substitution of Phe for Leu. As discussed, the opposite effects are seen in oxygen affinity and oxidation inhibition in rHb(*β*L28F) versus rHb(αL29F) (panels A and B of Figure 2 and Tables 1, 3, and 4). The difference in the functional properties must be a result of a variation in the detailed environment between the α-chain and *β*-chain distal heme pockets. Studies with Mbs have concluded that pocket size, steric hindrance, and H-bonding can affect ligand binding in the Tyr(B10) mutants (*44*). The distal heme pocket of the *β*-chain provides more room than the distal heme pocket of the α-chain (*2*, *3*, *45*, *46*). The greater distance from the positive edge of the phenyl ring multipole to the bound oxygen may inhibit favorable electrostatic interactions. As a result, the oxygen binding properties of rHb(*β*L28F) appear to be more similar to those of the Trp(B10) rHbs. Lack of favorable electrostatic interactions and steric hindrance could be the main factor affecting ligand binding for rHb(*β*L28F). In contrast, rHb(αL29F) is hypothesized to make electrostatic interactions between oxygen and the phenyl ring multipole (*12*, *14*, *17*). Another possible explanation for the different functional properties between rHb(αL29F) and rHb(*β*L28F) is that given more space in the *β*-chain distal heme pocket, bound oxygen can leave more easily despite the side chain of Phe already filling the pocket. Eich et al. (*15*) also offers an explanation for the difference in NO-induced oxidation rates between the α29Leu → Phe and *β*28Leu → Phe mutations in Hb based on modeling the components of the NO-induced oxidation reaction with the structure of the ethyl isocyanide complex of Hb A (*47*). Leu in the B10 position sterically hinders bound ethyl isocyanide on the α-chain but not the *β*-chain, where faster reactions involving isocyanides, NO, and oxygen take place (*48*). If Leu is more flexible on the *β*-chain, similar dynamics of Trp and Leu in rHb(*β*L28W) and rHb(*β*L28F) may allow oxygen to leave more easily (low oxygen affinity) and oxidation to occur faster than in rHb(αL29F).

^{1}H NMR studies on these rHbs with B10 mutations reveal the expected presence of various structural changes. As shown in Figure 3B, substitution of Trp or Phe for Leu in either the α- or *β*-chain of HbCO A perturbs the E11Val peak in the same chain, indicating significant changes in the tertiary structure of the distal heme pocket. Alterations to the distal heme pocket cause significant perturbations also in the corresponding proximal heme pocket in the deoxy form as seen in Figure 4A. A noticeable shift is seen for the α87His peak in rHb(αL29F) and rHb(αL29W), and the *β*92His peak shift for rHb(*β*L28F) and rHb(*β*L28W). These indications of considerable tertiary structural changes in the heme pocket appear to show a correlation with the major differences observed in oxygen binding and oxidation properties in these mutant rHbs versus those of Hb A.

The chemical shift of a nucleus is determined by its environment; therefore, the chemical shifts of various protons in a protein could in principle be calculated from its structure. TOTAL (*49*) calculates ^{1}H chemical shifts with reasonably good accuracy from a protein structure in Protein Data Bank format, allowing a comparison of resonances measured in solution with the values expected from a crystal structure (*50*). Recently, crystal structures for several B10 mutants have been deposited with the Protein Data Bank (entries 1O1I, 1O1J, 1O1L, 1J7S, and 1J7W). Unfortunately, they cannot be compared directly with our B10 mutants because the crystal structures have an additional mutation (αH58Q or *β*H63Q) at the E7 site, which is also in the distal heme pocket. Moreover, all but one of the structures are for the deoxy form. The only available ligated structure is for the cyanomet form, not CO. Figure 5 shows a comparison between the distal heme pockets of HbCO A (PDB entry 1IRD) and that of the triple mutant rHb(αV1M,αL29F,αH58Q) in the cyanomet form (PDB entry 1O1I). Under the assumption that this triple mutant is a good geometric model for our single-point mutant rHb(αL29F), we used TOTAL to calculate the expected chemical shift for the γ_2-E11Val methyl in Hb A and rHb(αV1M,αL29F,αH58Q). The fact that the crystal structure is for the paramagnetic, cyanomet-ligated form of Hb is not relevant to this comparison, since the program does not include the effects of paramagnetism in its calculation of chemical shifts. The result is −1.67 ppm for HbCO A and −1.62 ppm for the triple mutant. We observe values of −1.75 ppm for HbCO A and −2.01 ppm for rHbCO(αL29F). Figure 5 shows a clear difference in the position of the E11Val methyls between HbCO A and the triple mutant in the cyanomet form, yet the predicted chemical shifts are essentially the same. This result confirms that, although a change in chemical shift implies a change in the environment of the nucleus, the geometry may change while the chemical shift remains constant.

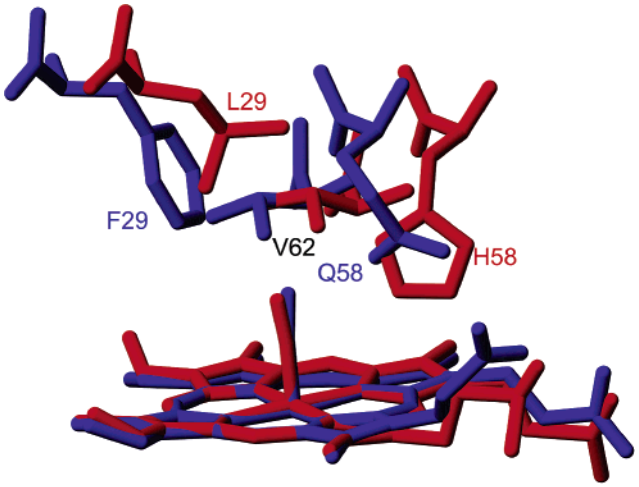

FIGURE 5: α-Subunit distal heme pocket of HbCO A (PDB entry 1IRD, colored red) and that of the triple mutant cyanomet-rHb(αV1M,αL29F,αH58Q) (PDB entry 1O1I, colored blue). The hemes of the two crystal structures have been superimposed, to emphasize the relative displacement of the mutated residues and αV62.

For the other B10 mutants, only crystal structures for the deoxy state are available. For protons near the paramagnetic iron, chemical shifts (if observable despite enhanced relaxation) are influenced by the distance to the iron as well as the angles between the Fe−^{1}H vector and axes of the paramagnetic tensor (*51*). All of these factors may change as the heme pocket geometry changes in response to mutations. The elements of the paramagnetic tensor are unknown for Hb A, the rHbs reported here, and the mutant Hbs for which crystal structures are available. Therefore, a meaningful comparison between observed and expected chemical shifts for deoxy-Hbs cannot be made.

The inspection of the NMR results indicates that the quaternary structure is slightly affected by the B10 mutations. The $\alpha_1\beta_1$ interface of the rHbs in the CO form remains very similar to that of Hb A as interpreted from Figure 3A. The $\alpha_1\beta_2$ interface of deoxy-rHb(αL29W), -rHb(βL28F), and -rHb(βL28W) does not change much with respect to the deoxy (T) markers of deoxy-Hb A at 14.1 and 11.2 ppm (Figure 4B). There is an upfield shift for both of the T-markers for rHb(αL29F), but this could be interpreted as a weakening of the H-bonds in the $\alpha_1\beta_2$ interface in this high-affinity mutant rather than a change in the structure. As the quaternary structure does not seem to undergo much change, the tetrameric structure of hemoglobin and its ability to perform conformational changes are preserved in these rHbs as evidenced by the good cooperativity and the Bohr effect data (Tables 1 and 2).

The results presented here provide new insight into designing rHbs with mutations in the distal heme pockets of the α- and β-chains as potential HBOCs or hemoglobin therapeutics. Most likely, rHb(αL29F) and rHb(αL29W) have the best qualities for these applications, especially considering oxidation inhibition (Tables 3 and 4). The ability to preserve Hb in the reduced, ferrous form is an important characteristic necessary to keep extracellular HBOCs or hemoglobin therapeutics functional in the absence of a natural met-Hb reductase system. The two α-chain mutant rHbs studied here could help reduce the degree of hypertension when using HBOCs, since the degree of hypertension appears to have a direct relationship with the NO-induced oxidation rates of extracellular hemoglobin (*16*). The low oxygen affinity with reasonable cooperativity found for rHb(αL29W), rHb(βL28F), and rHb(βL28W) is also favorable for extracellular HBOCs or hemoglobin therapeutics. Without allosteric effectors such as 2,3-BPG that lower the oxygen affinity inside red blood cells (*1*), rHbs with low oxygen affinity could release oxygen when necessary in the body. Overall, the best choice in view of these functional properties is rHb(αL29W) for its ability to combine low oxygen affinity with oxidation inhibition. It does not prevent autoxidation or NO-induced oxidation to the extent that the αL29F mutation does, but rHb(αL29W) exhibits a low oxygen affinity that could make it a better choice than rHb(αL29F) with its less desirable high oxygen affinity. In the future, another option for the study of these B10 mutant rHbs for HBOCs or hemoglobin therapeutics would be to create mutants that add additional single or multiple mutations at different locations to achieve simultaneously the desired properties of enhanced oxidation inhibition and low oxygen affinity.

In conclusion, considerable progress has been made in designing novel rHbs as potential HBOCs or hemoglobin therapeutics during the past 5 years. For recent reviews on this topic, see refs *52*−*56*. At present, there are three approaches to overcoming the hypertension effect due to nitric oxide scavenging by the first generation of HBOCs, i.e., (i) to make the tetrameric Hb bigger by either polymerization with glutaraldehyde-type reagents or conjugation with polyethylene glycol or *o*-raffinose, (ii) to make mutations in the distal heme pockets of the Hb molecule to reduce the reactivity of NO with Hb, and (iii) to combine both procedures. So far, these modified Hbs exhibit some undesirable properties, such as ease of oxidation, high oxygen affinity, low cooperativity, instability, etc., compared to Hb A. To overcome these shortcomings, we need to carry out a genetic engineering approach to design novel recombinant hemoglobins to overcome these undesirable properties. The results obtained from the four rHbs with mutations at the B10 positions of both the α- and β-chains of Hb A offer new encouragement for the design of the next generation of HBOCs.

ACKNOWLEDGMENT

We thank Dr. Seong Tae Jeong for constructing the plasmids for expressing recombinant hemoglobins with mutations in the distal heme pockets and Dr. Ching-Hsuan Tsai for advice in carrying out the stopped-flow experiments. We thank Dr. Ming F. Tam for carrying out mass spectrometric and Edman degradation analyses to assess the quality of our recombinant hemoglobins. We also thank Dr. E. Ann Pratt for helpful discussions.

REFERENCES

1. Dickerson, R. E., and Geis, I. (1983) *Hemoglobin: Structure, Function, Evolution, and Pathology*, pp 1−176, The Benjamin/Cummings Publication Co. Inc., Menlo Park, CA.
2. Shen, T.-J., Ho, N. T., Simplaceanu, V., Zou, M., Green, B. N., Tam, M. F., and Ho, C. (1993) Production of unmodified human adult hemoglobin in *Escherichia coli*, *Proc. Natl. Acad. Sci. U.S.A. 90*, 8108−8112.
3. Shen, T.-J., Ho, N. T., Zou, M., Sun, D. P., Cottam, P. F., Simplaceanu, V., Tam, M. F., Bell, D. A., Jr., and Ho, C. (1997) Production of human normal adult and fetal hemoglobins in *Escherichia coli*, *Protein Eng. 10*, 1085−1097.
4. Kim, H.-W., Shen, T.-J., Sun, D. P., Ho, N. T., Madrid, M., and Ho, C. (1995) A novel low oxygen affinity recombinant hemoglobin (α96Val→Trp): Switching quaternary structure without changing the ligation state, *J. Mol. Biol. 248*, 867−882.
5. Ho, C., Sun, D. P., Shen, T.-J., Ho, N. T., Zou, M., Hu, C.-K., Sun, Z.-Y., and Lukin, J. A. (1998) Recombinant hemoglobins with low oxygen affinity and high cooperativity, in *Present and Future Perspectives of Blood Substitutes* (Tsuchida, E., Ed.) pp 281−296, Elsevier Science SA, Lausanne, Switzerland.
6. Tsai, C.-H., Shen, T.-J., Ho, N. T., and Ho, C. (1999) Effects of substitutions of lysine and aspartic acid for asparagine at β108 and of tryptophan for valine at α96 on the structural and functional properties of human normal adult hemoglobin: Roles of $\alpha_1\beta_1$ and $\alpha_1\beta_2$ subunit interfaces in the cooperative oxygenation process, *Biochemistry 38*, 8751−8761.
7. Tsai, C.-H., Fang, T.-Y., Ho, N. T., and Ho, C. (2000) Novel recombinant hemoglobin, rHb (βN108Q), with low oxygen affinity, high cooperativity, and stability against autoxidation, *Biochemistry 39*, 13719−13729.
8. Jeong, S. T., Ho, N. T., Hendrich, M. P., and Ho, C. (1999) Recombinant hemoglobin (α29Leu→Phe, α96Val→Trp, β108Asn→Lys) exhibits low oxygen affinity and high cooperativity combined with resistance to autoxidation, *Biochemistry 38*, 13433−13442.
9. Tsai, C.-H., and Ho, C. (2002) Recombinant hemoglobins with low oxygen affinity and high cooperativity, *Biophys. Chem. 98*, 15−25.
10. Di Iorio, E. E., Winterhalter, K. H., Mansouri, A., Blumberg, W. E., and Peisach, J. (1984) Studies on the oxidation of hemoglobin Zurich (β63 E7 Arg), *Eur. J. Biochem. 145*, 549−554.
11. Ji, X., Karavitis, M., Razynska, A., Kwansa, H., Vásquez, G., Fronticelli, C., Bucci, E., and Gilliland, G. L. (1998) α-Subunit oxidation in T-state crystals of a sebacyl cross-linked human hemoglobin with unusual autoxidation properties, *Biophys. Chem. 70*, 21−34.
12. Carver, T. E., Brantley, R. E., Jr., Singleton, E. W., Arduini, R. M., Quillin, M. L., Phillips, G. N., Jr., and Olson, J. S. (1992) A novel site-directed mutant of myoglobin with an unusually high O_2 affinity and low autooxidation rate, *J. Biol. Chem. 267*, 14443−14450.

13. Brantley, R. E., Jr., Smerdon, S. J., Wilkinson, A. J., Singleton, E. W., and Olson, J. S. (1993) The mechanism of autooxidation of myoglobin, *J. Biol. Chem. 268*, 6995−7010.
14. Olson, J. S., Eich, R. F., Smith, L. P., Warren, J. J., and Knowles, B. C. (1997) Protein engineering strategies for designing more stable hemoglobin-based blood substitutes, *Artif. Cells, Blood Substitutes, Immobilization Biotechnol. 25*, 227−241.
15. Eich, R. F., Li, T., Lemon, D. D., Doherty, D. H., Curry, S. R., Aitken, J. F., Mathews, A. J., Johnson, K. A., Smith, R. D., Phillips, G. N., Jr., and Olson, J. S. (1996) Mechanism of NO-induced oxidation of myoglobin and hemoglobin, *Biochemistry 35*, 6976−6983.
16. Doherty, D. H., Doyle, M. P., Curry, S. R., Vali, R. J., Fattor, T. J., Olson, J. S., and Lemon, D. D. (1998) Rate of reaction with nitric oxide determines the hypertensive effect of cell-free hemoglobin, *Nat. Biotechnol. 16*, 672−676.
17. Dou, Y., Maillett, D. H., Eich, R. F., and Olson, J. S. (2002) Myoglobin as a model system for designing heme protein based blood substitutes, *Biophys. Chem. 98*, 127−148.
18. Hayashi, A., Suzuki, T., and Shih, M. (1973) An enzymic reduction system for metmyoglobin and methemoglobin, and its application to functional studies of oxygen carriers, *Biochim. Biophys. Acta 310*, 309−316.
19. Benesch, R. E., Benesch, R., and Yung, S. (1973) Equations for the spectrophotometric analysis of hemoglobin mixtures, *Anal. Biochem. 55*, 245−248.
20. Winterbourn, C. C., McGrath, B. M., and Carrell, R. W. (1976) Reactions involving superoxide and normal and unstable haemoglobins, *Biochem. J. 155*, 493−502.
21. Szebeni, J., Winterbourn, C. C., and Carrell, R. W. (1984) Oxidative interactions between haemoglobin and membrane lipid. A liposome model, *Biochem. J. 220*, 685−692.
22. Wallace, W. J., Houtchens, R. A., Maxwell, J. C., and Caughey, W. S. (1982) Mechanism of autooxidation for hemoglobins and myoglobins. Promotion of superoxide production by protons and anions, *J. Biol. Chem. 257*, 4966−4977.
23. Macdonald, V. W. (1994) Measuring relative rates of hemoglobin oxidation and denaturation, *Methods Enzymol. 231*, 480−490.
24. Zwart, A., Buursma, A., van Kampen, E. J., Oeseburg, B., van der Ploeg, P. H., and Zijlstra, W. G. (1981) A multi-wavelength spectrophotometric method for the simultaneous determination of five haemoglobin derivatives, *J. Clin. Chem. Clin. Biochem. 19*, 457−463.
25. Rohlfs, R. J., Bruner, E., Chiu, A., Gonzales, A., Gonzales, M. L., Magde, D., Magde, M. D., Jr., Vandegriff, K. D., and Winslow, R. M. (1998) Arterial blood pressure responses to cell-free hemoglobin solutions and the reaction with nitric oxide, *J. Biol. Chem. 273*, 12128−12134.
26. Plateau, P., and Guéron, M. (1982) Exchangeable proton NMR without base-line distortion using new strong-pulse sequences, *J. Am. Chem. Soc. 104*, 7310−7311.
27. Wyman, J., Jr. (1948) Heme proteins, *Adv. Protein Chem. 4*, 407−531.
28. Wyman, J., Jr. (1964) Linked functions and reciprocal effects in hemoglobin: A second look, *Adv. Protein Chem. 19*, 223−286.
29. Tsuruga, M., and Shikama, K. (1997) Biphasic nature in the autoxidation reaction of human oxyhemoglobin, *Biochim. Biophys. Acta 1337*, 96−104.
30. Tsuruga, M., Matsuoka, A., Hachimori, A., Sugawara, Y., and Shikama, K. (1998) The molecular mechanism of autoxidation for human oxyhemoglobin, *J. Biol. Chem. 273*, 8607−8615.
31. Suzuki, T., Watanabe, Y.-h., Nagasawa, M., Matsuoka, A., and Shikama, K. (2000) Dual nature of the distal histidine residues in the autoxidation reaction of myoglobin and hemoglobin: Comparison of the H64 mutants, *Eur. J. Biochem. 267*, 6166−6176.
32. Ho, C. (1992) Proton nuclear magnetic resonance studies on hemoglobin: Cooperative interactions and partially ligated intermediates, *Adv. Protein Chem. 42*, 153−312.
33. Russu, I. M., Ho, N. T., and Ho, C. (1987) A proton nuclear Overhauser effect investigation of the subunit interfaces in human normal adult hemoglobin, *Biochim. Biophys. Acta 914*, 40−48.
34. Simplaceanu, V., Lukin, J. A., Fang, T.-Y., Zou, M., Ho, N. T., and Ho, C. (2000) Chain-selective isotopic labeling for NMR studies of large multimeric proteins: Application to hemoglobin, *Biophys. J. 79*, 1146−1154.
35. Chang, C.-k., Simplaceanu, V., and Ho, C. (2002) Effects of amino acid substitutions at β131 on the structure and properties of hemoglobin: Evidence for communication between $\alpha_1\beta_1$ and $\alpha_1\beta_2$ subunit interfaces, *Biochemistry 41*, 5644−5655.
36. Fang, T.-Y., Simplaceanu, V., Tsai, C.-H., Ho, N. T., and Ho, C. (2000) An additional H-bond in the $\alpha_1\beta_2$ interface as the structural basis for the low oxygen affinity and high cooperativity of a novel recombinant hemoglobin (βL105W), *Biochemistry 39*, 13708−13718.
37. Lindstrom, T. R., Noren, I. B., Charache, S., Lehmann, H., and Ho, C. (1972) Nuclear magnetic resonance studies of hemoglobins. VII. Tertiary structure around ligand binding site in carbonmonoxyhemoglobin, *Biochemistry 11*, 1677−1681.
38. Dalvit, C., and Ho, C. (1985) Proton nuclear Overhauser effect investigation of the heme pockets in ligated hemoglobin: Conformational differences between oxy and carbonmonoxy forms, *Biochemistry 24*, 3398−3407.
39. Takahashi, S., Lin, A. K., and Ho, C. (1980) Proton nuclear magnetic resonance studies of hemoglobins M Boston (α58E7 His→Tyr) and M Milwaukee (β67E11 Val→Glu): Spectral assignments of hyperfine-shifted proton resonances and of proximal histidine (E7) NH resonances to the α and β chains of normal human adult hemoglobin, *Biochemistry 19*, 5196−5202.
40. La Mar, G. N., Nagai, K., Jue, T., Budd, D. L., Gersonde, K., Sick, H., Kagimoto, T., Hayashi, A., and Taketa, F. (1980) Assignment of proximal histidyl imidazole exchangeable proton NMR resonances to individual subunits in hemoglobins A, Boston, Iwate and Milwaukee, *Biochem. Biophys. Res. Commun. 96*, 1172−1177.
41. Fung, L. W.-M., and Ho, C. (1975) A proton nuclear magnetic resonance study of the quaternary structure of human homoglobins in water, *Biochemistry 14*, 2526−2535.
42. Perutz, M. F. (1970) Stereochemistry of cooperative effects in haemoglobin, *Nature 228*, 726−739.
43. Ishimori, K., Imai, K., Miyazaki, G., Kitagawa, T., Wada, Y., Morimoto, H., and Morishima, I. (1992) Site-directed mutagenesis in hemoglobin: Functional and structural role of inter- and intrasubunit hydrogen bonds as studied with 37β and 145β mutations, *Biochemistry 31*, 3256−3264.
44. Draghi, F., Miele, A. E., Travaglini-Allocatelli, C., Vallone, B., Brunori, M., Gibson, Q. H., and Olson, J. S. (2002) Controlling ligand binding in myoglobin by mutagenesis, *J. Biol. Chem. 277*, 7509−7519.
45. Shaanan, B. (1983) Structure of human oxyhaemoglobin at 2.1 Å resolution, *J. Mol. Biol. 171*, 31−59.
46. Derewenda, Z., Dodson, G., Emsley, P., Harris, D., Nagai, K., Perutz, M., and Renaud, J.-P. (1990) Stereochemistry of carbon monoxide binding to normal human adult and Cowtown haemoglobins, *J. Mol. Biol. 211*, 515−519.
47. Johnson, K. A. (1993) X-ray structures of myoglobin and hemoglobin-alkylisocyanide complexes, Ph.D. Dissertation, Rice University, Houston, TX.
48. Mathews, A. J., and Olson, J. S. (1994) Assignment of rate constants for O_2 and CO binding to α and β subunits within R- and T-state human hemoglobin, *Methods Enzymol. 232*, 363−386.
49. Williamson, M. P., and Asakura, T. (1993) Empirical comparisons of models for chemical shift calculation in proteins, *J. Magn. Reson., Ser. B 101*, 63−71.
50. Lukin, J. A., Simplaceanu, V., Zou, M., Ho, N. T., and Ho, C. (2000) NMR reveals hydrogen bonds between oxygen and distal histidines in oxyhemoglobin, *Proc. Natl. Acad. Sci. U.S.A. 97*, 10354−10358.
51. Bertini, I., Luchinat, C., and Parigi, G. (2002) Magnetic susceptibility in paramagnetic NMR, *Prog. Nucl. Magn. Reson. Spectrosc. 40*, 249−273.
52. Haney, C. R., Buehler, P. W., and Gulati, A. (2000) Purification and chemical modifications of hemoglobin in developing hemoglobin based oxygen carriers, *Adv. Drug Delivery Rev. 40*, 153−169.
53. Winslow, R. M. (2003) Current status of blood substitute research: Towards a new paradigm, *J. Intern. Med. 253*, 508−517.
54. Chang, T. M. (2003) Future generations of red blood cell substitutes, *J. Intern. Med. 253*, 527−535.

55. Alayash, A. I. (2004) Oxygen therapeutics: Can we tame haemoglobin? *Nat. Rev. 3*, 152−159.
56. Olson, J. S., Foley, E. W., Rogge, C., and Tsai, A.-L. (2004) NO scavenging and the hypertensive effect of hemoglobin-based blood substitutes, *Free Radical Biol. Med. 36*, 685−697.
57. Koradi, R., Billeter, M., and Wüthrich, K. (1996) MOLMOL: A program for display and analysis of macromolecular structures, *J. Mol. Graphics 14*, 51−55.

BI048289A